Applied Catalysis B: Environmental 132–133 (2013) 469–478

Contents lists available at SciVerse ScienceDirect

Applied Catalysis B: Environmental

journal homepage: www.elsevier.com/locate/apcatb

Decomposition of methane over unsupported porous nickel and alloy catalyst

Aik Chong Lua*, Hong Yan Wang

School of Mechanical and Aerospace Engineering, Nanyang Technological University, 50 Nanyang Avenue, Singapore 639798, Republic of Singapore

ARTICLE INFO

Article history:
Received 5 September 2012
Received in revised form
12 December 2012
Accepted 14 December 2012
Available online 21 December 2012

Key words:
Nickel catalyst
Nickel-copper catalyst
Unsupported catalyst
Methane decomposition
Hydrogen production
Carbon nano-fibre

ABSTRACT

Unsupported NiO and NiO-CuO nano-particles were prepared by a facile method and these nano-particles showed promising catalytic activity towards methane decomposition. The decomposition of fibrous nickel (or mixed) oxalate precursors led to the formation of porous oxide aggregates with small primary oxide particles of 8–20 nm. Similar to supported catalysts, nickel–copper alloy particles showed steady catalytic activities even at high reaction temperatures (>700 °C). Unlike the supported catalysts, it was necessary to introduce methane to the reactor at lower temperatures to avoid catalyst particles sintering into bigger ones during the reaction. The initial carbon nano-fibres (CNFs) acted as living supports to take the catalyst particles away and prevent them from sintering with adjacent particles. The textural properties of the CNFs were characterized by transmission electron microscopy (TEM), X-ray diffraction (XRD) and N_2 adsorption. The textural and micro-structural properties depended on the composition of the catalyst and the reaction temperature.

1. Introduction

Presently, concerns over environmental effects of energy use, in the form of global warming, ozone layer depletion and acid rains, have led to intense research on the exploration of clean energy. Hydrogen is widely considered to be one of the most promising, alternative energy carriers and clean fuels. Hence, much research has focused on the development of efficient, low cost and environmental friendly methods for hydrogen production [1]. Among the many hydrogen production reactions, the catalytic decomposition of methane (CDM) over catalysts has generated much interest [2]. The methane decomposition reaction,

$$CH_4 \rightarrow C + 2H_2, \Delta H_{298}^{\circ} = 75.6\,\text{kJ/mol} \quad (1)$$

is a moderately endothermic reaction which is thermodynamically favoured at higher temperature. CDM is a green route to produce hydrogen with carbon nanotubes (CNTs) or carbon nanofibres (CNFs) as the only side product. This will eliminate the need for CO_x separation and sequestration processes altogether. It was found that transition 3d-metals (Fe, Co, Ni) show considerable catalytic activity towards dissociation of hydrocarbon [2]. On one hand, their non-filled 3d-orbitals can accept electrons from hydrocarbon molecules which facilitate the dissociation. On the other hand, the overlap of non-filled 3d-orbitals with carbon orbital will not only favour the hydrocarbon dissociation process but will also play an important role in the initial stage of the CNTs or CNFs growth [3].

In general, for CDM reactions, Ni-based catalysts are more active than Co-based and Fe-based catalysts in the temperature range 500–700 °C [4,5]. Therefore, supported metallic nickel catalysts for CDM has attracted much attention [2,6–19]. There is a consensus in the literature that the catalyst performance in CDM is highly dependent on the crystallite size of the catalyst particles. Larger crystallite or particle size would render the catalyst to be deactivated rapidly. Normally, support materials such as Al_2O_3, SiO_2, MgO are used to control the catalyst particle size and dispersion by physical interactions (porous support) or chemical interaction (charge transfer effect) [3]. Martínez-Arias and co-workers [20] studied the support effect of Ni-Cu/CeO_2 catalyst for its catalytic activity towards methane oxidation and decomposition as well as its reduction activity. Their results showed that Gd-doped support would promote the formation of Ni-Cu alloy with greater homogeneous composition, higher CH_4 oxidation and similar methane decomposition activities when compared with using CeO_2 as support.

It had been reported that unsupported pure nickel was inactive for the CDM process as these large polycrystalline particles (500–1000 nm) showed no catalytic activity [21,22]. Few studies have focused on the catalytic activity of unsupported catalyst for the CDM although bulk catalyst may offer some advantages

* Corresponding author.
E-mail address: maclua@ntu.edu.sg (A.C. Lua).

0926-3373/$ – see front matter © 2012 Elsevier B.V. All rights reserved.
http://dx.doi.org/10.1016/j.apcatb.2012.12.014

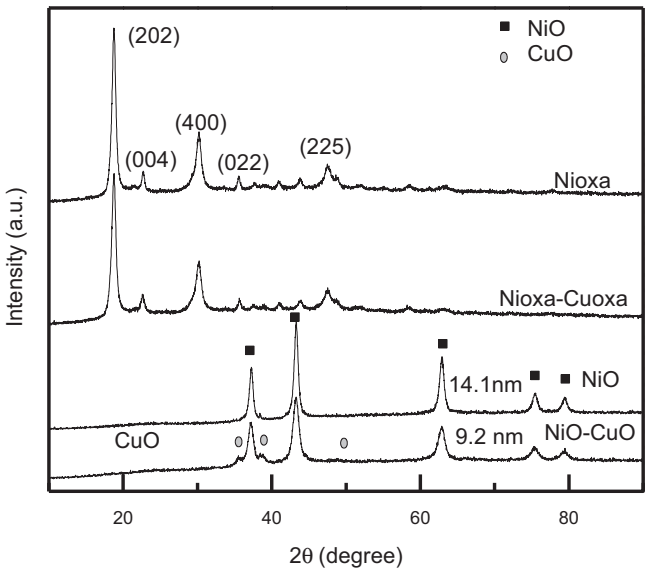

Fig. 1. XRD patterns of the samples Nioxa, Nioxa-Cuoxa, NiO and NiO-CuO. (The crystal sizes of the metal oxides were calculated from the most intense peak at around 43°).

over supported catalyst. Unsupported catalyst, for instance, may prevent the formation of traceable CO via the reaction of the carbonaceous residues with the oxygen in the support, like SiO_2 and Al_2O_3 [6,8,23]. Moreover, the bulk nickel catalyst could provide easy recovery of the catalyst and a convenient way for the purification of the CNFs by leaching the bulk metal catalyst with a mild acid solution [24] or simply using a magnetic field [25].

The magnetic property of Ni nanostructures has been extensively examined in terms of size and shape but its catalytic property is less understood. This is probably due to the insufficient thermal stability of these nickel nanomaterials under the reaction conditions [26]. In the present work, the application of mesoporous metal oxide (NiO or NiO-CuO) as catalyst for methane decomposition is reported. The thermal decomposition of nickel oxalate or mixed metal oxalate would result in their respective mesoporous oxides with nano-sized primary particles (8–20 nm) which could further be reduced into active Ni and Ni-Cu alloy catalysts for the thermal decomposition of methane. These Ni and Ni-Cu alloy particles were used as unsupported CDM catalysts in which the textural and micro-structural properties were also studied.

2. Experimental

2.1. Catalyst preparation

Metal oxide nano-particles were synthesized by the decomposition of metal oxalate [27]. In a typical procedure for preparing nickel oxide or nickel oxide-cupric oxide, 2.6 g Ni $(NO_3)_2{\cdot}6H_2O$ or 2.6 g $Ni(NO_3)_2{\cdot}6H_2O$ and 0.72 g $Cu(NO_3)_2{\cdot}3H_2O$ (with 3:1 Ni/Cu atomic ratio) was dissolved into 30 ml of pure ethanol. A stoichiometric amount of oxalic acid, dissolved in 30 ml pure ethanol, was titrated to the above solution using a burette under magnetic stirring for 30 min. The light blue suspension was transferred into a 100 ml capacity Telfon-lined stainless steel autoclave and kept at 120 °C for 12 h. After cooling to room temperature, a bluish solid precipitate was obtained by filtration and then thoroughly washed with distilled water. The resulting precipitate was dried at 80 °C under vacuum. The dried samples would be denoted as Nioxa and Nioxa-Cuoxa. Then, they were calcined in a quartz tube reactor at 500 °C for 2 h under oxygen flow to obtain the final products: NiO and NiO-CuO.

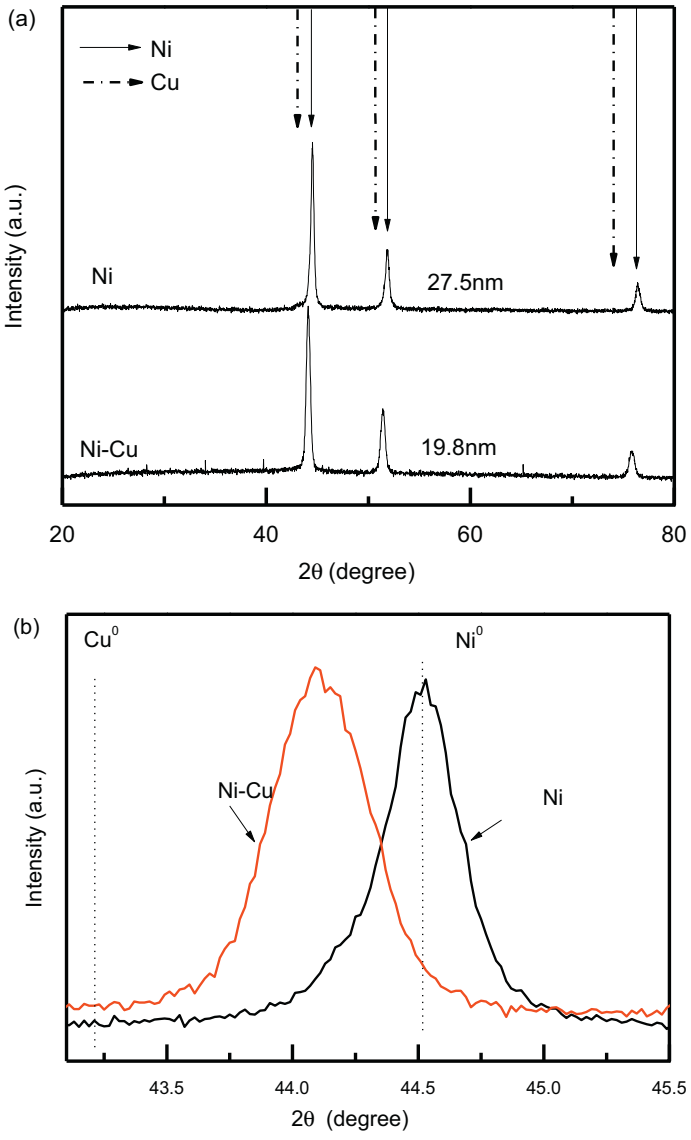

Fig. 2. XRD patterns of the Ni and Ni-Cu samples after reduction in H_2. The crystal sizes were calculated from the most intense peak of metallic Ni or Ni-Cu alloy. The bottom graph (b) shows the expanded region corresponding to the most intense peaks of the Ni and Ni-Cu alloy along with the positions expected for the pure metals.

2.2. Characterization

In order to characterize the freshly prepared reactive nickel catalyst, a passivation treatment was conducted to avoid self-ignition of the nickel catalyst. After the nickel oxide particles were reduced in the quartz tube reactor, it was subsequently cooled down to ambient temperature in a nitrogen atmosphere. Then, a slightly oxidizing O_2–N_2 mixture stream consisting of 0.5% O_2 was allowed to flow through the prepared metallic nickel particles for 1 h at room temperature before the sample was removed from the reactor.

Powder X-ray diffraction (XRD) patterns were measured by an X-ray diffractometer (Philips, PW1830) using CuKα ($\lambda = 1.5406$ Å) radiation at 40 kV and 30 mA and operated on a continuous scan mode. The X-ray diffraction patterns were recorded in the scan range of $2\theta = 10$–$90°$ at a scan rate of 1°/min. Scherrer equation, employing the most intense diffraction peak in each case, was used to determine the crystal size, whereby the particle shape factor was taken as 0.9.

Nitrogen adsorption–desorption isotherms of the catalysts were determined at 77 K on a volumetric adsorption analyzer

(Micromeritics, ASAP 2020). The surface area of the nickel particles was calculated using the multipoint BET equation. Pore size distributions were calculated by the BJH method using the adsorption branch of the isotherm.

Field emission scanning electron microscopy (FESEM) was used to study the morphology and the physical characteristics of the metallic nickel particle catalyst and the deposited carbon using a field emission scanning electron microscope (JEOL JSM-7600F) with a resolution of 1 nm (15 kV), equipped with an energy dispersive X-ray spectroscopy (EDX).

Transmission electron microscopy (TEM) micrographs were obtained using a transmission electron microscope (JEOL JEM 2010) with a 0.23 nm point resolution at an operating voltage of 200 kV. Samples for the TEM analysis were prepared by drying the catalyst particles in ethanol on carbon-coated copper grids.

Temperature-programmed reduction (TPR) measurements were carried out using a TPR system (Quantachrome ChemBET 3000). Typically, about 0.03 g of catalyst sample (NiO or NiO-CuO) was placed in a U-tube holder and the sample was first degassed at 300 °C for 2 h by flushing with N_2 gas. Upon degassing, the reductive gas mixture consisting of 5% H_2/95% N_2 at a flow rate of 50 ml/min flowed through the sample. The sample was heated from ambient conditions to 1000 °C to obtain the TPR profiles of the sample.

2.3. Catalytic reaction

Methane decomposition experiments were conducted in a long quartz tube reactor (ID 10 mm, length 800 mm) which was heated by an electric furnace (Lenton, LTF/12/28/500) under atmospheric pressure. 50 mg of NiO or NiO-CuO was placed in the centre of the quartz tube reactor and the sample was supported on quartz wool. A K-type thermocouple covered with a quartz thermo-well was placed near the catalyst bed to detect the temperature of the catalyst bed. The reactor was vertically fitted in the electric furnace. Before the reaction, a reduction treatment of the catalysts was performed – the reactor temperature was first increased to 400 °C under N_2 flow of 50 ml min^{-1}. Then, 5% H_2 in N_2 was introduced to the reactor and the temperature was kept at 400 °C for 1 h. The reduced catalysts of NiO and NiO-CuO would be denoted as Ni or Ni-Cu respectively. Subsequently, the temperature was increased to the reaction temperature (500–750 °C) under N_2 gas (route I) or CH_4-N_2 gas (route II). For route I, methane was only introduced to the reactor when it had reached the desired reaction temperature. N_2 was used as the gas atmosphere during the temperature-rise period. In route II, methane was introduced to the reactor immediately after the reduction reaction and continued to flow throughout the subsequent temperature ramp-up period and the decomposition reaction. The reaction conditions for all the catalysts were as follows: a catalyst charge of 50 mg and a total flow rate of 25 ml/min with methane concentration of 20% for a range of reaction temperatures from 500 to 750 °C. The outflow gas after the reactor was analyzed by a gas chromatograph (Agilent 6890-5973 GC-MS network system) which was equipped with a HP-molesieve column and a TCD detector using helium as the carrier.

3. Results and discussion

3.1. Characterization of the precursors and catalysts

Nickel and copper oxalates were used as precursors for producing nickel and copper oxides, respectively. Nickel oxalate dihydrate ($NiC_2O_4{\cdot}2H_2O$) belongs to the magnesium series (Mg, Mn, Fe, Co, Ni and Zn) which can crystallize into the α form (monoclinic) or β form (orthorhombic) depending on the preparation conditions [28]. Usually, the oxalates contain two structural water molecules, for instance, $NiC_2O_4{\cdot}2H_2O$. Copper oxalate hydrate does not belong to the magnesium series and different water contents are proposed in the published articles ($CuC_2O_4{\cdot}xH_2O$, $0 < x < 1$, e.g. $x = 1/3$, $1/2$) [29–31].

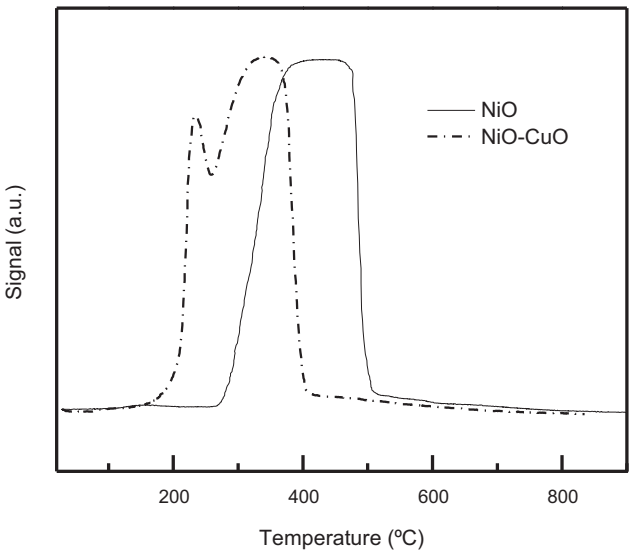

Fig. 3. Temperature-programmed reduction curves of NiO and NiO-CuO.

Fig. 1 shows the XRD patterns of the prepared catalyst precursors before and after calcination. All the diffraction peaks of the nickel oxalate or nickel-copper oxalate precursors showed the characteristics of the nickel oxalate hydrate phase which could be indexed to the orthorhombic phase of $NiC_2O_4{\cdot}2H_2O$ (JCPDS 25-0582). After calcination in air, a series of distinct diffraction peaks at $2\theta = 37$, 44, 62, 75 and 79° were also observed which corresponded to NiO (JCPDS 44-1159). CuO reflections were also observed in the NiO-CuO sample indicating that the solid solution of NiO and CuO was not formed completely, leaving remnant CuO particle inclusions intact.

XRD patterns of the samples after reduction treatment under 5% H_2–95% N_2 flow at 400 °C are shown in Fig. 2. Three prominent reflections which could be assigned to metallic Ni planes (1 1 1), (2 0 0) and (2 2 0) were evident in the pure nickel catalyst. In the Cu containing sample, Ni-Cu alloy was formed from the evidence of a slight shift in the position of the metallic Ni peaks which were located between the positions of pure metallic nickel and metallic copper as shown in Fig. 2(b). The lattice parameter of Ni-Cu alloy was 3.556 Å which corresponded to a Ni:Cu atomic composition close to 2.33:1 [32]. However, the atomic ratio of Ni/Cu as determined by EDX was about 2.95:1, which was closer to the nominal ratio of 3:1. The slight enrichment in the Cu as determined from the lattice parameter was in agreement with a slightly longer delay in nickel reduction as shown in the TPR test in Fig. 3. Martinez-Arias and co-workers [20] proposed that in the reduction process of supported NiO-CuO, the delay in the nickel reduction (a higher reduction temperature) as compared with copper probably led to the formation of a core slightly enriched in Cu and a surface enriched in nickel.

To be active in the decomposition reaction, catalysts must be in the metallic state. The reduction characteristics of NiO and NiO-CuO were studied by TPR as shown in Fig. 3. The reduction curve of pure NiO had one peak and it commenced to be reduced at about 390–450 °C. The curve of NiO-CuO shows two peaks – a small sharp one centred at 230 °C and a large one with its maximum reduction peak rate at round 340 °C. An in situ study [33] reported that CuO could be rapidly reduced and the presence of metallic Cu could greatly enhance the reducibility of the Ni species. It was proposed

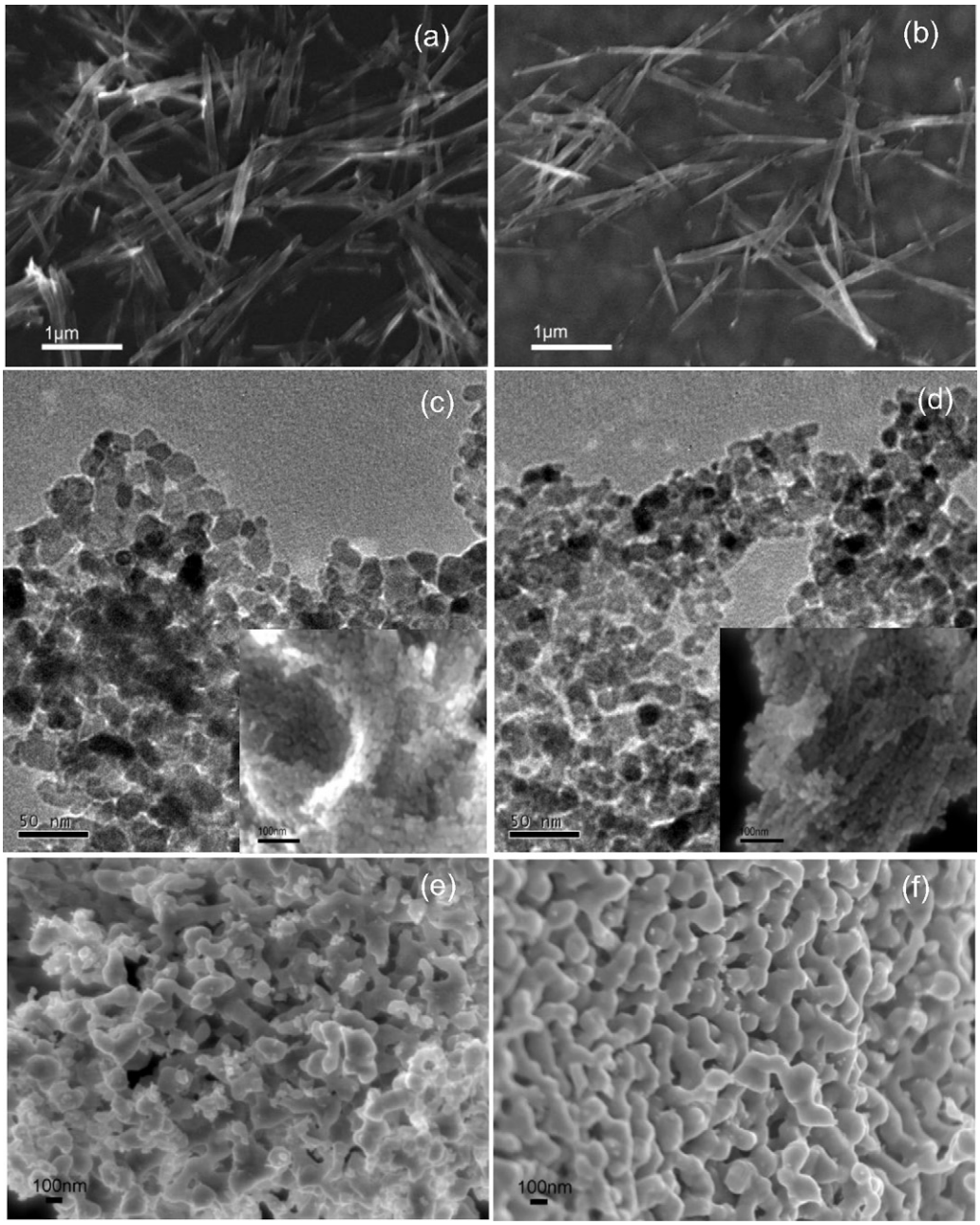

Fig. 4. FESEM micrographs of catalyst precursors and reduced catalysts: (a) Nioxa, (b) Nioxa-Cuoxa, (c) NiO (inset), (d) NiO-CuO (inset), (e) Ni, (f) Ni-Cu alloy and TEM micrographs of (c) NiO and (d) NiO-CuO.

[34] that metallic copper can dissociate the hydrogen molecule into hydrogen atoms which can be spilled over to the surface of the neighbouring NiO. This led to a lower NiO reduction temperature as compared with that of pure NiO. Therefore, in the curve of NiO-CuO, the first peak at the lower temperature was attributed to the reduction of Cu ($Cu^{II} \rightarrow Cu^{0}$) while the other one was the reduction of NiO [35,36]. In addition, the reduction temperature was dependent on the particle size. For bulk NiO or Co_3O_4, it was reported that for smaller particle size, the initial reduction temperature would be lower [37,38]. So, the lower reduction temperature of NiO-CuO might be attributed to its smaller particle sizes (Fig. 4(c) and (d)) or the crystallite size (9.2 nm for NiO-CuO in comparison to 14.1 nm for NiO). In the case of the NiO-CuO, the complete reduction to the metallic alloy was accomplished at a temperature of about 400 °C while for the NiO, the complete reduction to nickel was achieved at a temperature of about 500 °C. In the supported nickel based catalyst systems, such as Ni-Cu/Al_2O_3, Ni-Cu/MgO, high reduction temperature, typically about 700 °C is needed because of the strong interaction between nickel and its support [39,40]. In this study, with unsupported catalyst, a much lower reduction temperature of 400 °C was sufficient.

Fig. 4 shows the morphologies and particle sizes of the oxalate precursors, metal oxides and metallic nickel and alloy. Fig. 4(a) and (b) shows that the nickel oxalate and nickel-copper oxalate respectively have rod-like morphology. The fibre-like oxalate structures were decomposed into aggregates of spherically shaped particles of NiO and NiO-CuO in the presence of oxygen as shown in Fig. 4(c) and (d) respectively. Fig. 5(a) and (b) compares the particle size distributions of NiO and NiO-CuO which were based on the TEM micrographs by counting about 100 primary particles. The pore size distributions of NiO and NiO-CuO aggregates are shown in Fig. 5(c) and (d) which were based on N_2 adsorption isotherms at 77 K. As

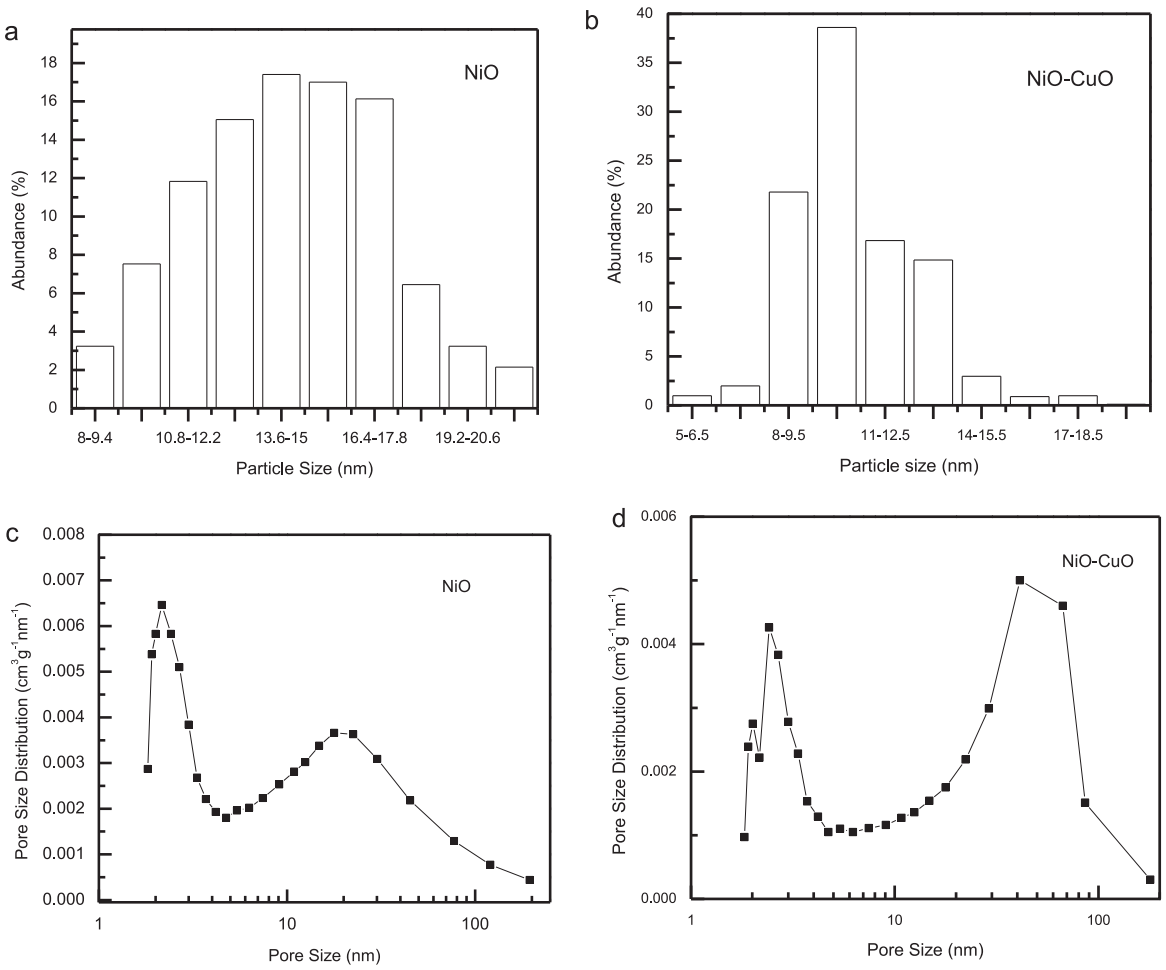

Fig. 5. Particle size distributions (a, b) and pore size distributions (c, d) of NiO and NiO-CuO.

shown in Fig. 5, both NiO and NiO-CuO had wide particle size and wide pore size distributions. However, for NiO-CuO, the particle size distribution was more normal with a distinct dominant size centring at around 9.5–11 nm (Fig. 5(b)) as compared with that of NiO, with sizes ranging from 13.6 to 17.8 nm (Fig. 5(a)). The particle size ranges of NiO-CuO and NiO as determined by TEM were in good agreement with the crystal sizes as derived from the XRD patterns which were 9.2 and 14.1 nm respectively (Fig. 1). A bimodal pore size distribution was observed for both NiO and NiO-CuO particles. The first peak probably corresponded to the size of cavities between adjacent primary particles as deduced from Fig. 4(c) and (d). The second peak corresponded to the mesopores and macropores existing in the NiO or NiO-CuO aggregates. The surface areas of NiO and NiO-CuO were 60 and 40 cm^3/g respectively.

After reduction of NiO and NiO-CuO by H_2, the primary small nickel and nickel-copper crystallites tended to coalesce and agglomerate together, resulting in large nickel and nickel-copper particle aggregates. As shown in Fig. 4(e) and (f), the metallic nickel or Ni-Cu particles were joined together and grown into bigger particles. In comparison with the metallic Ni, the reduced Ni-Cu alloy would tend to form continuous networks as shown in Fig. 4(e), which was probably due to the linking of the agglomerates of Ni-Cu particles.

3.2. Catalytic activity

Fig. 6(a) and (b) shows the methane conversion and hydrogen formation rate over nickel catalysts as a function of reaction time using routes I and II respectively. It appeared that both routes resulted in the same trend: at 500 °C, the nickel catalyst yielded stable catalytic activity which was relatively higher for route II. However, the catalyst lost its activity when the decomposition temperature was increased to 550 °C. At this reaction temperature of 550 °C, the Ni catalyst deactivated faster using route I than route II with the deactivation durations lasting about 125 min and 275 min respectively.

The catalytic activity of methane decomposition over unsupported Ni-Cu catalyst was studied for varying reaction temperatures. Similar to the reactions with Ni catalyst, two reaction processes, i.e., routes I and II were studied. Fig. 7(a) and (b) shows the methane conversion and hydrogen formation rate over Ni-Cu catalysts as a function of reaction time using routes I and II respectively. Comparing Ni-Cu catalyst with nickel catalyst at 500 °C reaction temperature, the hydrogen formation rate was lower due to the reduction of active sites on the particle surface. However, the reaction temperature had increased to study higher temperatures than those for Ni catalyst. Fig. 7(b) shows that increasing reaction temperature greatly increased the methane conversion rate as the reaction is endothermic. However, for reaction temperature above 750 °C, the Ni-Cu catalyst deactivated rapidly probably due to the breakdown of the catalyst to a quasi-liquid state as evidenced by the TEM micrographs which would be discussed in the next section. Due to pressure buildup, the tests for 700 and 750 °C reaction temperatures were carried out for shorter durations as shown in Fig. 7(b).

At a reaction temperature of 600 °C in Fig. 7(a), the Ni-Cu catalyst subjected to route I was deactivated and lost its catalytic activity completely after a short duration as compared with those

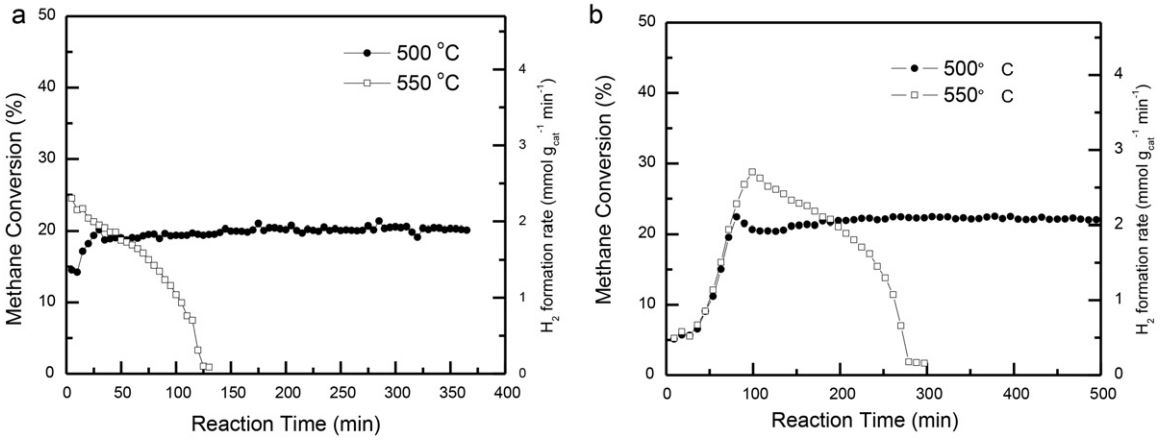

Fig. 6. Catalytic activity tests of Ni catalysts using (a) route I and (b) route II.

at 500 and 550 °C. However, for the Ni-Cu catalyst prepared using route II, the catalyst remained active even up to 750 °C with a highest methane conversion of 85%. Fig. 8(a) and (b) shows the TEM micrographs of Ni-Cu catalyst at the initial stage at 600 °C using routes I and II respectively. It clearly showed that the Ni-Cu particles prepared using route I sintered and coalesced into much larger particles when compared with catalyst using route II. The initial resulting carbons produced are surmised to play the role of "supports" to stabilize and disperse the catalyst particles as shown in Fig. 8(b). Fig. 8(c) shows the same catalyst using route I after the reaction at 600 °C. The catalyst was deactivated which could be attributed to the carbon deposits on the catalyst surfaces. A comparison of this morphology with that of the catalyst at the initial stage in Fig. 8(a) showed that the deposited carbon covered the catalyst surface in Fig. 8(c).

3.3. Characterization of the deposited carbon

Fig. 9 shows the used Ni catalysts using route II at reaction temperatures of 500 °C and 550 °C. At a reaction temperature of 500 °C, fibre-like carbons were produced with faceted Ni particles on the tips. One Ni particle gave rise to one smooth and regular shaped carbon filament with a diameter of about 100 nm. However, at 550 °C, two types of carbon co-existed. One type consisted of very fine carbon fibre with diameters of about 10–50 nm (Fig. 9(c)). Another type appeared as large lumps of carbon fibres with large nickel particles of 100–200 nm embedded inside (Fig. 9(d)).

The commonly accepted model of methane decomposition and carbon growth on nickel catalysts consists of three stages: (1) activation and decomposition of methane on Ni(1 0 0) and Ni(1 1 0) planes, (2) carbon dissolution and diffusion through the catalyst particle, (3) carbon segregation in the form of CNFs or CNTs on Ni(1 1 1) planes due to the coincidental symmetry between the Ni (1 1 1) and graphite (0 0 2) [2,3]. To maintain the continuous growth of CNFs, the balance among the methane decomposition rate, the carbon diffusion rate and the precipitation rate has to be achieved by using appropriate catalyst particle size [41]. At higher temperature, the decomposition rate is higher due to the endothermic nature of the reaction. At the same time, the unsupported nickel particles may be sintered into bigger particles. The balance is broken when the dissociation rate is much faster than the carbon diffusion rate and subsequently carbon layers will be formed on the active surfaces of the catalysts, resulting in the so-called deactivation process. Only small catalyst particles can be active for this higher temperature reaction as shown in Fig. 9(c). It also can be explained that although the catalyst particles in Fig. 9(b) and (d) had comparable sizes (100–150 nm), the catalyst particles in Fig. 9(d) became deactivated due to carbon capsulation at a higher temperature of 550 °C.

In the case of the Ni-Cu catalyst, the range of the reaction temperatures had been extended up to 750 °C, i.e., from 500 °C to 750 °C as shown in Fig. 7(b). The TEM micrographs of the used Ni-Cu catalysts are shown in Fig. 10. During the reaction as shown in Fig. 10(a)–(e), all the Ni-Cu catalysts had been sintered into quasi-octahedral particles whose particle size could reach up to

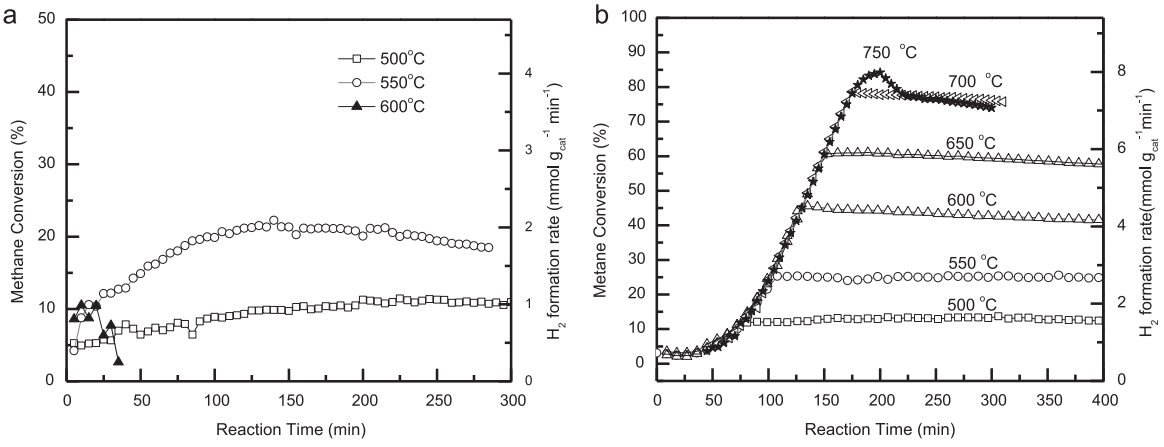

Fig. 7. Catalytic activity tests of Ni-Cu catalysts using (a) route I and (b) route II.

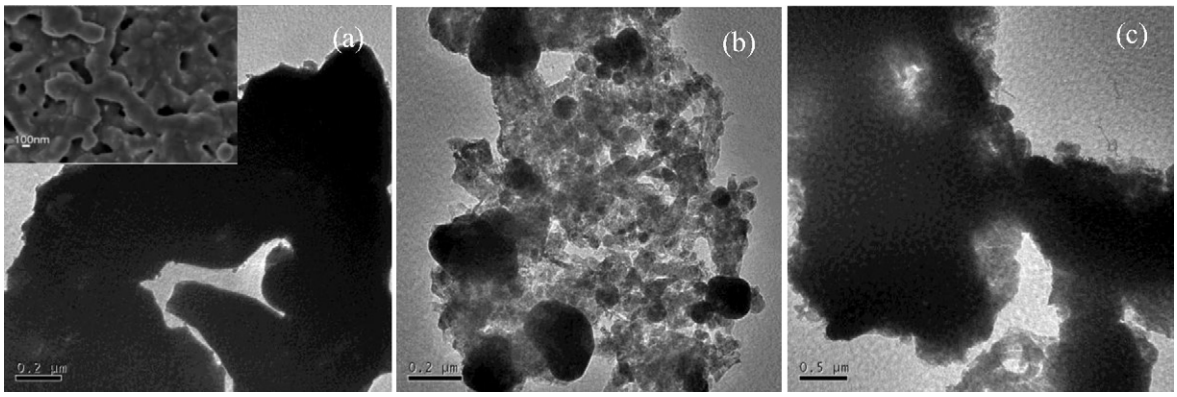

Fig. 8. TEM micrographs of metallic Ni-Cu alloy at the initial stage at 600 °C using (a) route I, inset (FESEM micrograph), and (b) route II. TEM micrograph (c) of the deposited carbon after the decomposition reaction using route I.

300–400 nm. Several filaments grew from one particle to form the "octopus" structure which was fully consistent with the observations on supported Ni-Cu catalysts. The doping effect of copper has been studied and can be summarized into two aspects: diluting the active sites of nickel (1 0 0 and 1 1 0) for dissociation of methane and promoting more precipitation sites (1 1 1) for carbon filament formation [2,42,43]. Copper itself is inactive for methane decomposition. Introducing copper to nickel will definitely decrease methane decomposition rate. Copper segregation on the alloy surface into island-like sectors is characteristic of the Ni-Cu system [44,45]. The copper segregation on the Ni (1 1 1) planes results in the formation of several carbon filaments growing from one particle which facilitates carbon transportation. In moderate temperature range, for instance from 500 to 700 °C in the tests in Fig. 10(a)–(e), the carbon diffusion and precipitation rates are able to keep pace with the methane decomposition rate. However, in the Ni-Cu system, a temperature limit exists, above which, some of the Ni-Cu alloy particles would become a quasi-liquid state and part of the catalyst particles might be sucked deep into the interior of the carbon filament or bamboo-shaped CNT such as those shown in Fig. 10(f) and (h) (see the circled areas). This migration is apparently due to the so-called catalyst periodical jumping mechanism. In this action, the quasi-liquid catalyst particle can be easily split into smaller particles and lose its catalytic activity. The reaction temperature used was much lower than the metal melting points. Bulk copper has a melting point of 1083 °C, which is much lower than that of nickel (1453 °C) [46]. The melting point of Ni-Cu alloy usually falls between their respective individual melting values. Therefore, the existence of the metal in a quasi-liquid state at about 750 °C is probably attributed to the size effect of nano-metal particles [47,48] and the interfacial effect between nano-carbon and nano-metal [9,48]. Therefore, the occurrence of a quasi-liquid state of the catalyst depends on the particle size, composition, metal support interaction [9], and the interfacial wetting effect by the carbon during reaction. Hence, some of the larger particles can still be rigid and less of a liquid state as shown in Fig. 10(g) and (h) (see square area).

Upon careful examination, it was revealed that the microstructure and textural characteristics of the carbon deposit depended on the constituents of the catalyst and the reaction temperature. The CNFs generated using pure nickel in Fig. 9 showed ordered and smooth structure whose surface area was also relatively lower than that of Ni-Cu catalyst as shown in Table 1. The addition of copper in the Ni-Cu catalyst led to CNFs with disordered and coarse structure, having a great number of mesopores on the surface (Fig. 10(a)–(d)). However, when the reaction temperature was increased to 700 or 750 °C, the surface of the CNF turned out to be smooth which seems to be related to the surface composition of the catalyst. Wang and Baker [49] prepared a series of Ni-Cu-MgO catalysts with high catalytic activity and stability at 665–725 °C. In contrast, Ni-MgO exhibited negligible activity at temperatures greater than 650 °C. In an earlier study [45], it was found that, in Ni-Cu system, copper could tend to segregate on the surface of the Ni-Cu alloy particle. As the methane was being introduced, there was an enhancement in the number of surface Ni^0 sites due to the selective and strong interaction between methane and nickel. Then, a balance was established between the carbon growth and its bulk diffusion at the regions. The existence of excessive number of exposed Ni^0 sites was indicated as the reason behind the fast deactivation in Ni-MgO. Metallic Ni diluted with Cu is less active than pure Ni for methane dissociation under a lower temperature (e.g. 500 °C). Besides, different from active Ni with half filled 3d shell, Cu,

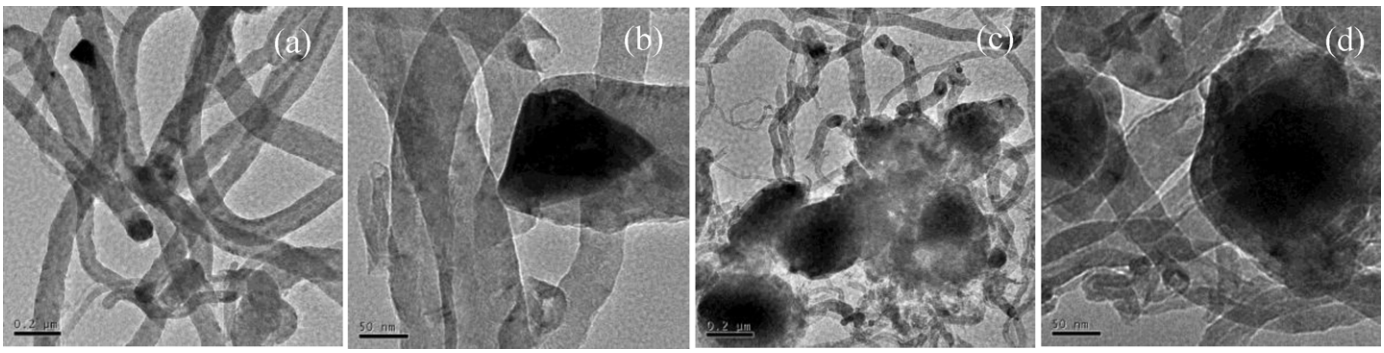

Fig. 9. TEM micrographs of carbon deposits on the Ni catalysts using route II at a reaction temperature of (i) 500 °C at (a) low magnification, and (b) high magnification; and (ii) 550 °C for (c) fine carbon fibres, and (d) lumps of carbon fibres. All the pictures presented are representative of the whole samples.

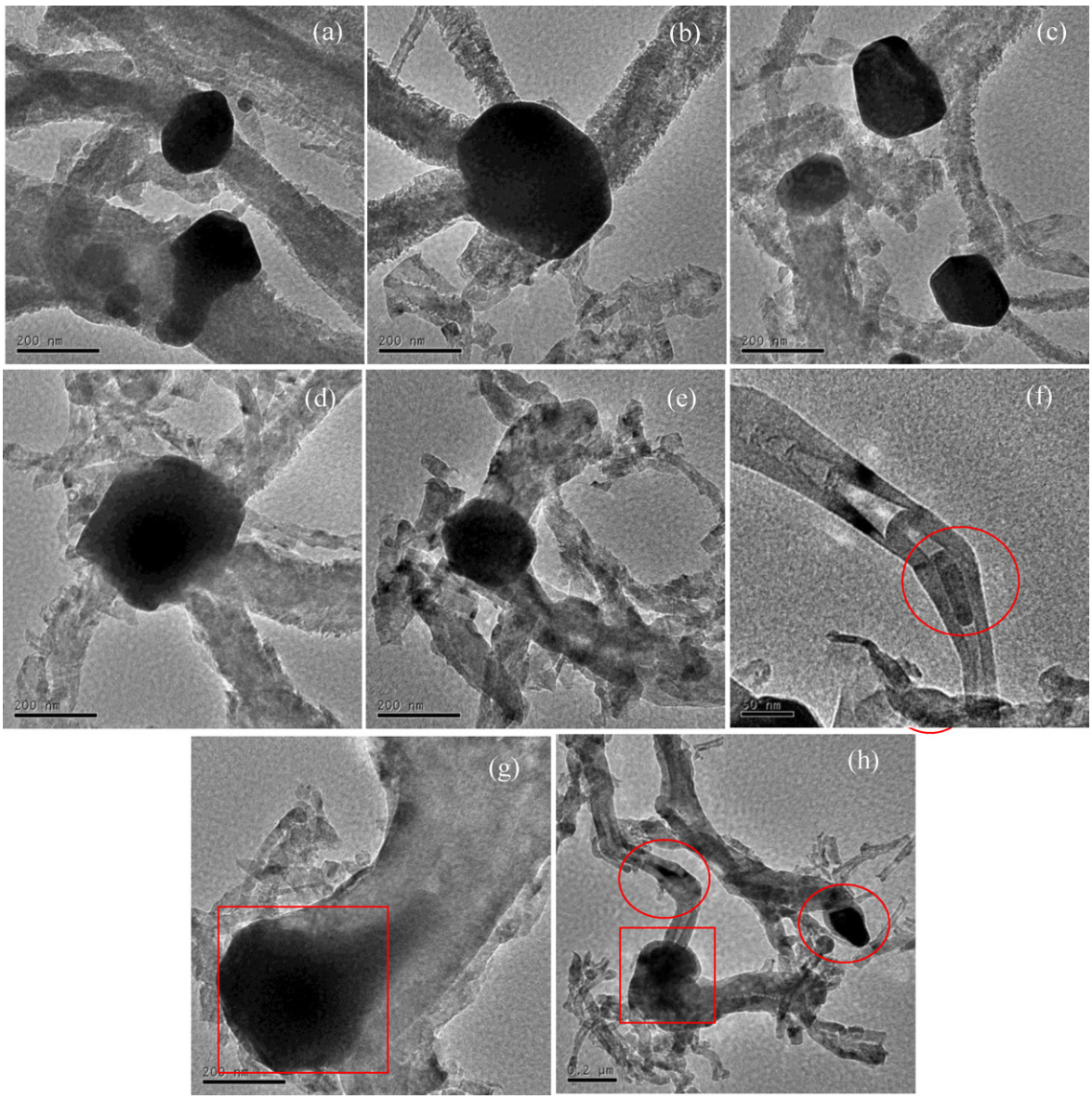

Fig. 10. TEM micrographs of carbon deposits on the Ni-Cu catalysts using route II at a reaction temperature of (a) 500 °C, (b) 550 °C, (c) 600 °C, (d) 650 °C, (e) 700 °C, and (f–h) 750 °C. All the pictures presented are representative of the whole samples.

a non-transition metal with its 3d shell completely filled, may exert electronic effects on Ni, thereby weakening the catalytic efficiency of the segregated nickel in alloy. In terms of carbon nucleation, it is likely that the presence of copper which can be uniformly dispersed or in the form of clusters in the bulk and on the surface of the catalyst particle, may influence the nucleation of the CNFs by blocking carbon dissolution in nickel [50]. Therefore, every nucleated carbon fibre possesses a porous structure with interstices in the bulk of the fibre. However, at high reaction temperature such as 750 °C, the copper and nickel may undergo a phase separation.

Table 1
Textural and structural characteristics of catalyst and carbon nano-fibres obtained from route II.

Sample	Catalyst	Carbon				
	[a] S_{BET} (m^2/g)	Temperature (°C)	S_{BET} (m^2/g)	V_{pore} (cm^3/g)	d_{002} (nm)	L_c (nm)
Ni	18.4	500	33.3	0.078	0.3410	6.1
Ni		550	45.2	0.135	0.3417	5.8
Ni-Cu	12.6	500	176.8	0.24	0.3413	5.3
Ni-Cu		550	171.6	0.294	0.3402	6.3
Ni-Cu		600	170.6	0.251	0.3393	7.4
Ni-Cu		650	107.8	0.169	0.3384	8.6
Ni-Cu		700	104.5	0.201	0.3387	9.5
Ni-Cu		750	108.4	0.289	0.3389	10.3

[a] S_{BET}(m^2/g): surface area of the catalyst after reduction in hydrogen.

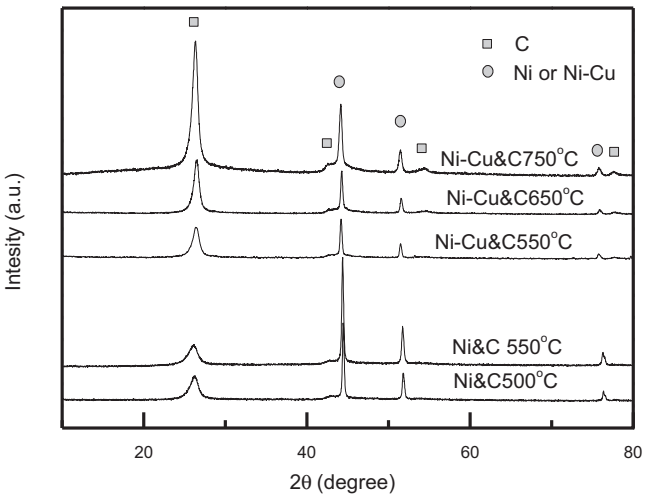

Fig. 11. XRD patterns of spent catalysts using route II under different reaction temperatures.

The copper element dispersed on the catalyst particle surface could reduce or become negligible, resulting in the formation of the carbon becoming uniform and smooth on the surface, similar to those generated from pure nickel.

The structural and textural properties of CNFs formed on Ni and Ni-Cu catalysts at 500–750 °C were studied using nitrogen adsorption and XRD analysis. XRD patterns of the selected carbon deposits revealed the presence of graphitic carbon, metallic Ni or Ni-Cu alloy as shown in Fig. 11. The results had been analyzed and summarized in Table 1. It could be seen that the introduction of copper essentially influenced the texture of the CNFs as exhibited by increases in the BET surface area and pore volume as compared with CNFs formed on the Ni catalyst [43,51]. The surface area of the CNF produced by the Ni-Cu catalyst at the lower temperatures of 500–600 °C had the highest value of about 170 m^2/g. However, further increase in the reaction temperature decreased the surface area of the resulting CNFs.

Interplanar distance d_{002} and the domain crystalline size L_c (along the *c*-axis which is directed perpendicular to the graphite plane (0 0 2)) of the CNFs were determined from XRD data. Table 1 shows that the structural parameters of CNFs depended on the temperature of methane decomposition. Generally, increasing the reaction temperature from 500 °C to 750 °C decreased the value of d_{002} from 0.341 to 0.338 nm which was approaching to that of perfect graphite (d_{002} = 0.3354 nm). However, the crystalline size L_c increased with increasing reaction temperature for CNFs produced using Ni-Cu catalyst.

4. Conclusions

Unsupported NiO and NiO-CuO particles with promising catalytic activity for methane decomposition were prepared by a facile method. Without support, the decomposition of fibrous oxalate precursors resulted in the formation of porous oxide aggregates (surface area of 40–60 m^2/g) with small primary particles (8–20 nm). These porous oxide aggregates required significant lower temperature in the reduction to become metallic state as compared with that of the supported ones as observed from the TPR results. After reduction, the porous metallic Ni or Ni-Cu alloy could become an effective catalyst for methane decomposition to produce hydrogen.

After the reduction of the metallic oxide to its metallic state at 400 °C, two process routes were investigated and the results showed that for the unsupported catalyst, it was vital to introduce methane to the reactor at lower temperature to avoid the catalysts from sintering into bigger particles. The initial CNFs acted as transporting agents and supports to take individual catalyst particles away and prevent them from sintering with adjacent particles. The unsupported Ni catalyst showed stable activity at a reaction temperature of 500 °C whereas the unsupported Ni-Cu catalyst exhibited stable activity for a wider temperature range of 500–750 °C. Like the supported catalyst, the addition of copper could shift the optimum temperature to 700 °C for the Ni-Cu catalyst due to the diluting effect to the active nickel sites although the particle size had increased as compared with the Ni catalyst. "Doping" copper led to the formation of "octopus" and porous CNFs, whose surface area was much higher than the one produced from pure Ni catalyst. However, at higher temperatures of 650–750 °C, the porous texture of CNFs was depressed probably due to the Ni-Cu alloy undergoing phase separation with increasing temperature. The XRD showed that increasing reaction temperature resulted in decreasing d_{002} and increasing average coherent scattering region directly perpendicular to the graphite plane (0 0 2) (L_c) of CNFs.

References

[1] R.M. Navarro, M.A. Pena, J.L.G. Fierro, Chemical Reviews 107 (2007) 3952–3991.
[2] Y.D. Li, D.X. Li, G.W. Wang, Catalysis Today 162 (2011) 1–48.
[3] A.C. Dupuis, Progress in Materials Science 50 (2005) 929–961.
[4] N.Z. Muradov, T.N. Veziroglu, International Journal of Hydrogen Energy 30 (2005) 225–237.
[5] Y. Zhang, K.J. Smith, Catalysis Letters 95 (2004) 7–12.
[6] Y. Li, B. Zhang, X. Tang, Y. Xu, W. Shen, Catalysis Communications 7 (2006) 380–386.
[7] Y. Echegoyen, I. Suelves, M.J. Lázaro, M.L. Sanjuán, R. Moliner, Applied Catalysis A 333 (2007) 229–237.
[8] T.V. Choudhary, C. Sivadinarayana, C.C. Chusuei, A. Klinghoffer, D.W. Goodman, Journal of Catalysis 199 (2001) 9–18.
[9] J. Chen, Y. Qiao, Y. Li, Applied Catalysis A 337 (2008) 148–154.
[10] J. Ashok, S.N. Kumar, M. Subrahmanyam, A. Venugopal, Catalysis Letters 118 (2007) 139–145.
[11] W. Zhang, Q.J. Ge, H.Y. Xu, Journal of Physical Chemistry A 114 (2010) 3818–3823.
[12] H.F. Abbas, W. Daud, International Journal of Hydrogen Energy 35 (2010) 1160–1190.
[13] Y.F. Sun, Z.J. Sui, J.H. Zhou, P. Li, X.G. Zhou, D. Chen, Asia-Pacific Journal of Chemical Engineering 4 (2009) 814–820.
[14] X.L. Zhu, D.G. Cheng, P.Y. Kuai, Energy and Fuels 22 (2008) 1480–1484.
[15] M.J. Lázaro, Y. Echegoyen, C. Alegre, I. Suelves, R. Moliner, J.M. Palacios, International Journal of Hydrogen Energy 33 (2008) 3320–3329.
[16] N. Latorre, J.I. Villacampa, T. Ubieto, E. Romeo, C. Royo, A. Borgna, A. Monzon, Topics in Catalysis 51 (2008) 158–168.
[17] J. Ashok, G. Raju, P.S. Reddy, M. Subrahmanyam, A. Venugopal, International Journal of Hydrogen Energy 33 (2008) 4809–4818.
[18] W. Gac, A. Denis, T. Borowiecki, L. Kepinski, Applied Catalysis A-General 357 (2009) 236–243.
[19] A. Venugopal, S. Naveen Kumar, J. Ashok, D. Hari Prasad, V. Durga Kumari, K.B.S. Prasad, M. Subrahmanyam, International Journal of Hydrogen Energy 32 (2007) 1782–1788.
[20] A. Hornes, P. Bera, M. Fernandez-Garcia, A. Guerrero-Ruiz, A. Martinez-Arias, Applied Catalysis B: Environmental 111 (2012) 96–105.
[21] M.L. Toebes, J.H. Bitter, A.J. van Dillen, K.P. de Jong, Catalysis Today 76 (2002) 33–42.
[22] Y.D. Li, J.L. Chen, L. Chang, Applied Catalysis A-General 163 (1997) 45–57.
[23] P. Ferreira-Aparicio, I. Rodríguez-Ramos, A. Guerrero-Ruiz, Applied Catalysis A 148 (1997) 343–356.
[24] Y. Li, B. Zhang, X. Xie, J. Liu, Y. Xu, W. Shen, Journal of Catalysis 238 (2006) 412–424.
[25] P. Jana, V.A.D. O'Shea, J.M. Coronado, D.P. Serrano, International Journal of Hydrogen Energy 35 (2010) 10285–10294.
[26] Y. Li, Q.Y. Liu, W.J. Shen, Dalton Transactions 40 (2011) 5811–5826.
[27] X. Wang, J.M. Song, L.S. Gao, J.Y. Jin, H.G. Zheng, Z.D. Zhang, Nanotechnology 16 (2005) 37–39.
[28] A. Angermann, J. Töpfer, Journal of Materials Science 43 (2008) 5123–5130.
[29] A. Michalowicz, J.J. Girerd, J. Goulon, Inorganic Chemistry 18 (1979) 3004–3010.
[30] H. Fichtnerschmittler, Crystal Research and Technology 19 (1984) 1225–1230.
[31] J. Romann, J.-C. Valmalette, V. Chevallier, A. Merlen, Journal of Physical Chemistry C 114 (2010) 10677–10682.
[32] L. Durivault, O. Brylev, D. Reyter, M. Sarrazin, D. Belanger, L. Roue, Journal of Alloys and Compounds 432 (2007) 323–332.
[33] P. Li, J. Liu, N. Nag, P.A. Crozier, Journal of Catalysis 262 (2009) 73–82.
[34] T.H. Chang, F.C. Leu, Journal of the Chemical Society, Faraday Transactions 92 (1996) 2291–2296.

[35] Y. Li, J. Chen, L. Chang, Y. Qin, Journal of Catalysis 178 (1998) 76–83.
[36] M.D. Cangiano, M.W. Ojeda, A.C. Carreras, J.A. Gonzalez, M.D. Ruiz, Materials Characterization 61 (2010) 1135–1146.
[37] Y.G. Ji, Z. Zhao, A.J. Duan, G.Y. Jiang, J. Liu, Journal of Physical Chemistry C 113 (2009) 7186–7199.
[38] H.S. Roh, H.S. Potdar, K.W. Jun, J.W. Kim, Y.S. Oh, Applied Catalysis A-General 276 (2004) 231–239.
[39] A. Monzon, N. Latorre, T. Ubieto, C. Royo, E. Romeo, J.I. Villacampa, L. Dussault, J.C. Dupin, C. Guimon, M. Montioux, Catalysis Today 116 (2006) 264–270.
[40] L. Dussault, J.C. Dupin, C. Guimon, M. Monthioux, N. Latorre, T. Ubieto, E. Romeo, C. Royo, A. Monzon, Journal of Catalysis 251 (2007) 223–232.
[41] R.T. Yang, J.P. Chen, Journal of Catalysis 115 (1989) 52–64.
[42] L.B. Avdeeva, O.V. Goncharova, D.I. Kochubey, V.I. Zaikovskii, L.M. Plyasova, B.N. Novgorodov, S.K. Shaikhutdinov, Applied Catalysis A 141 (1996) 117–129.
[43] T.V. Aapg BulletinReshetenko, L.B. Avdeeva, Z.R. Ismagilov, A.L. Chuvilin, V.A. Ushakov, Applied Catalysis A 247 (2003) 51–63.
[44] T.S. Cale, J.T. Richardson, Journal of Catalysis 79 (1983) 378–389.
[45] N.M. Rodriguez, M.S. Kim, R.T.K. Baker, Journal of Catalysis 140 (1993) 16–29.
[46] A. Moisala, A.G. Nasibulin, E.I. Kauppinen, Journal of Physics-Condensed Matter 15 (2003) S3011–S3035.
[47] K.J. MacKenzie, O.M. Dunens, A.T. Harris, Industrial and Engineering Chemistry Research 49 (2010) 5323–5338.
[48] Y.D. Li, J.L. Chen, Y.M. Ma, J.B. Zhao, Y.N. Qin, L. Chang, Chemical Communications (1999) 1141–1142.
[49] H.Y. Wang, R.T.K. Baker, Journal of Physical Chemistry B 108 (2004) 20273–20277.
[50] C.A. Bernardo, I. Alstrup, J.R. Rostrup-Nielsen, Journal of Catalysis 96 (1985) 517–534.
[51] V.B. Fenelonov, A.Y. Derevyankin, L.G. Okkel, L.B. Avdeeva, V.I. Zaikovskii, E.M. Moroz, A.N. Salanov, N.A. Rudina, V.A. Likholobov, S.K. Shaikhutdinov, Carbon 35 (1997) 1129–1140.